Eng. Sci., 2025, **36**, 1678

Engineered Science
DOI: https://dx.doi.org/10.30919/es1678

A Feasible Mechanochemical Ball Milling Method for Preparing Persulfate Activator for Tetracycline Degradation

Li Zhang,* Kang Li, Simiao Chen, Lijun Xu, Jianming Zhu, Qing Huang and Wenyi Yuan

Abstract

The use of activated persulfate to degrade antibiotics has been proven to be an effective technique. However, this technology requires the preparation of many nanoscale persulfate activators to adapt to engineering applications, which is still a challenge at present. In addressing the issue, this work prepared a nanoscale composite of pyrite@activated carbon (named FeS_2@AC) by mechanochemical ball milling. The composite has been shown to effectively activate persulfate, generating sulfate radicals ($SO_4^{-\bullet}$) and hydroxyl radicals ($OH^{\bullet}$). The optimal reaction conditions were determined through orthogonal experiments, range analysis, and variance analysis. At initial concentrations of 50 mg/L and 100 mg/L, the degradation rates of tetracycline hydrochloride by FeS_2@AC reached 87.28% and 85.62%, respectively. Combining experimental validation and density functional theory (DFT) calculations, Fe^{2+} serves as the primary catalytic site, while S^- species facilitate rapid Fe^{3+}/Fe^{2+} cycling, enhancing radical generation and catalytic durability. Notably, this one-step ball milling approach offers a cost-effective, scalable, and environmentally benign alternative to traditional nanomaterial synthesis methods. The study further elucidated degradation pathways and intermediate toxicity, providing critical insights for practical implementation. These findings present a transformative framework for engineering high-activity nanocatalysts to combat antibiotic pollution in wastewater treatment.

Keywords: Mechanochemical ball milling; Pyrite; Activation; Degradation; Tetracycline hydrochloride.
Received: 18 July 2025; Revised: 06 August 2025; Accepted: 07 August 2025.
Article type: Research article.

1. Introduction

Antibiotics such as tetracycline hydrochloride (TC) have become prevalent in numerous sectors including animal husbandry due to their extensive antimicrobial spectrum.[1-4] Literatures confirm that tetracycline hydrochloride has a limited ability to be absorbed and degraded in humans and animals, with 30% to 90% of the total amount of intake excreted in its original form through urine and feces,[5-8] which in turn enters the water environment,[9,10] exacerbating the problem of antibiotic contamination in the ecosystem.[11-14] At present, treatment strategies for antibiotics in water bodies are divided into three main categories: physical, chemical and biological method.[15-19] Due to the solubility of tetracycline in water, physical methods such as coagulation and precipitation are not effective.[20] Biological methods rely on the metabolic function of microorganisms to degrade low concentrations of antibiotics. However, this method is greatly affected by environmental conditions, and antibiotics may have inhibitory effects on microbial growth.[21] The effective removal of tetracycline from organic wastewater has become a major problem that needs to be overcome.

In recent years, there has been great interest in using advanced oxidation processes (AOPs) to degrade tetracycline. Photocatalysis is only suitable for treating low concentration pollutants, and the degradation efficiency is usually low for pollutants with concentrations of 100 mg/L and above. The Fenton method generates a large amount of iron sludge, which can easily cause catalyst deactivation and secondary pollution. In nowadays, the activation of persulfate (PS) to degrade pollutants has aroused widespread interests. The persulfate emerges as a chemical entity with notable oxidative properties, possessing a persulfate anion that is capable of direct reaction with a broad spectrum of organic compounds to achieve oxidative degradation.[22] Especially, activated persulfate exhibits a stronger oxidative capacity and can cope with more difficult to degrade organic compounds, significantly enhancing the oxidation efficiency.[23] The current methods for PS activation primarily encompass physical energy input activation (photoactivation, thermal activation, and ultrasonic

School of Resources and Environmental Engineering, Shanghai Polytechnic University, No.2360 Jinhai Road, Shanghai 201209, China
**Email*: zhangli@sspu.edu.cn (L. Zhang)

activation) and chemical catalytic activation (Metal-based catalysts, carbon materials, and metal organic frameworks (MOFs) materials.[24] Physical energy input activation promotes PS decomposition through external energy input, without the need for catalysts, but with high energy consumption and equipment costs, and difficult large-scale applications. In chemical catalytic activation methods, carbon materials such as activated carbon and graphene have attracted attention due to their low cost and ease of modification. However, the catalytic efficiency of raw carbon materials is relatively low, and their performance needs to be improved by doping (such as nitrogen, sulfur) or loading metals (such as Fe, Co). This also increases its usage cost; MOFs have excellent efficiency but high cost, especially MOF materials are difficult to store for a long time and are prone to structural collapse, which affects the reusability. Metal based catalysts include homogeneous catalysts and heterogeneous catalysts. Traditional homogeneous catalysts (such as Fe^{2+}) have low costs, but are prone to deactivation and lead to iron sludge precipitation. Heterogeneous catalysts such as Co_3O_4, CuO_2, *etc*. reduce the reaction energy barrier through surface adsorption and activation PS, and are recyclable and stable. However, the heterogeneous catalysts usually need to be prepared as nanomaterials to increase the number of active sites. Although this improves catalytic efficiency, the preparation process of nanomaterials usually requires high energy consumption, and nanomaterials are prone to reduce activity due to agglomeration.[25-29] The combination of heterogeneous catalysts with carbon materials to create nanoscale composite catalysts has aroused widespread interest. Heterogeneous catalysts compensate for the insufficient activity of carbon materials, and the use of carbon materials can also save metal resources. Moreover, the larger specific surface area of carbon materials is conducive to the dispersion of heterogeneous catalysts and reduces agglomeration. A series of heterogeneous catalyst/carbon composite materials, including Fe@AC (copper alginate), porous copper alginate/graphene oxide (CA/GO), nitrogen-doped porous charcoal-loaded zero-valent iron (Fe-NPC), and magnetically reduced graphene oxide nanosheets-iron oxide (rGO-Fe_3O_4) have been synthesized.[30-33] However, the preparation process of these materials is relatively complex and the preparation conditions are harsh. If highly active composite materials can be prepared directly from natural minerals and activated carbon using simple methods, it will effectively promote the engineering application of advanced oxidation technology for degrading antibiotic wastewater.

Mechanochemical ball milling technology has been extensively studied in the field of metal material preparation, as well as in related areas such as mechanical alloying, inorganic material preparation, mineral material activation, and nanocomposite material preparation.[34,35] The mechanochemical ball milling method is not only a simple and efficient way to prepare ultrafine nanoparticles, but also relatively inexpensive. The heat generated during the mechanochemical ball milling process endows the material with unique properties.[36-39] Preparing nanoscale iron ore-activated carbon composites by mechanochemical methods for persulfate activation, offer a novel approach for the treatment of antibiotic wastewater.[40] FeS_2, as the main component of natural mineral pyrite, is a green and low-cost PS activating substance. By combining FeS_2 with activated carbon through mechanochemical ball milling, not only can metal/non-metal composite materials be efficiently prepared, but the obtained ultrafine particles are expected to improve the activation efficiency of persulfate. However, to the best of our knowledge, the reports on the preparation of iron ore-activated carbon nanocomposites by mechanochemical ball milling to active PS and to investigate their degradation effects on tetracycline are still relatively limited.

In this work, we successfully synthesized nanocomposites of iron ore (FeS_2) and activated carbon using mechanochemical ball milling (named as FeS_2@AC). Compared with existing PS activation technologies, our synthesized materials have cheaper raw materials, simpler preparation methods, and lower costs. The combination of nanoscale FeS_2 catalyst and carbon material has improved its catalytic efficiency. After five cycles of use, the activity loss rates were only 10.06% and 10.34%, respectively. Compared with the existing superior PS activators, the FeS_2@AC combining the recyclability and surface catalytic activity of heterogeneous catalysts, a balance between cost, efficiency, and stability has been achieved, providing a more practical option for PS activation.

2. Experimental section

2.1 Materials

Tert-butanol ($C_4H_{10}O$, $\geq$ 99.5%, AR) was purchased from Sinopharm Chemical Reagent Co. Sodium persulfate ($Na_2S_2O_8$, $\geq$ 99.0%, AR), tetracycline hydrochloride ($C_{22}H_{25}ClN_2O_8$, 97%, HPLC), ascorbic acid ($C_6H_8O_6$, 99%, BR), sodium nitrite ($NaNO_2$, 99.99%, RG), pyrite (FeS_2, 99.9%, RG), activated charcoal (AC, 99%, 200 mesh, RG), and disodium ethylene diamine tetraacetic acid ($C_{10}H_{12}N_2Na_2O_8$, $\geq$ 98%, RG) were purchased from Shanghai Taitan Technology Co.

2.2 Preparation of composites by ball milling method

Firstly, 0.45 g of FeS_2 and 0.45 g of AC were added into a 50 mL zirconium dioxide ball mill jar. Subsequently, the nitrogen flow rate was adjusted to a suitable level and maintained for 5 min to eliminate the risk of powder eruption inside the jar and to exhaust the residual air thoroughly. The ball milling jars are sealed with a rubber ring, the lid is tightly fastened and the mouth of the jars is reinforced with black tape to connect the lid to ensure a tight seal. Following this, the ball milling jar was placed in a planetary ball mill, with the ball-to-material ratio set at 80:1 and the rotational speed set at 500 rpm for a period of 4 min. Following the conclusion of the ball milling process, the powder was promptly removed and sealed for storage in a dry tray.

2.3 Activation degradation experiment

FeS_2@AC activated PS degradation of tetracycline: 50 mg/L and 100 mg/L tetracycline hydrochloride solutions were pre-configured, mixed thoroughly and placed in a backlit place for use. Sodium persulfate (11.9 mg) was added to 50 ml of tetracycline hydrochloride solution, and following complete dissolution, FeS_2@AC (5.0 mg) was introduced to initiate the reaction. The pH was adjusted to 3 using 0.5 mol/L HCl and NaOH, and ultrasonication was carried out for 1 min to disperse agglomerated particles in the powder of FeS_2@AC. At 5 min intervals, 2 ml of samples were taken, and the samples were filtered using a 0.22 μm filter head and then analyzed using a UV spectrophotometer to detect the concentration of tetracycline hydrochloride. The intermediates were analyzed by using Shimadzu LCMS-8040.

Tetracycline hydrochloride removal rate was calculated according to Eq. (1):

$$D = \frac{C_0 - C}{C_0} \times 100\% \tag{1}$$

where D: tetracycline hydrochloride removal rate, 100%; C_0: initial concentration of tetracycline hydrochloride, mg/L; C: tetracycline hydrochloride concentration, mg/L.

In the subsequent phase of the study, the impact of various parameters on the degradation of tetracycline hydrochloride was investigated. These parameters included the ball milling time, the ball milling speed, the ball-to-material ratio, the composite concentration, the sodium persulfate concentration, and the initial pH. Orthogonal experiments were conducted to ascertain the optimal conditions for the degradation of tetracycline hydrochloride by FeS_2@AC.

2.4 Experimental characterization

The X-ray diffraction patterns of the samples were obtained using a X-Pert PRO MPD model X-ray diffractometer, with a Cu-Kα-ray source (wavelength λ = 1.5418 Å). The microscopic morphology of the samples was characterized in detail by a scanning electron microscope (SEM) model S-4800 with a transmission electron microscope (TEM) model JEM-2100F. Concurrently, the elemental composition and elemental chemistries of the samples were analyzed by ESCALAB 250XI model electron spectrometer (XPS). The free radical species were explored by using sodium nitrite, tert-butanol and ascorbic acid as free radical trapping agents, and the ESR spectra were recorded by a Bruker EMXplus model electron paramagnetic resonance spectrometer (ESR). This allowed the free radical species that were activated and played a major role in the degradation of tetracycline hydrochloride to be identified.

2.5 Density functional theory (DFT) calculation

The DFT calculations for FeS_2 were performed using the Vienna Ab initio Simulation Package (VASP) code with the projector-augmented-wave method and the Perdew-Burke-Ernzerhof functional including Grimme's DFT-D3 dispersion corrections.[41-43] We employed a kinetic energy of 500 eV in plane-wave basis sets. FeS_2 (100) slab based on 2 × 2 × 1 supercells of the crystal structures with 20-Å vacuum along the c axis. The calculations with the FeS_2 (100) slab also applied the Hubbard U corrections (U = 1.50 eV, J = 0 eV).

The adsorption energy (E_{binding}) is calculated following Eq. (2):

$$E_{binding} = E_{mol+slab} - E_{mol} - E_{slab} \tag{2}$$

where $E_{\text{mol+slab}}$ represents the total energy of the molecule adsorbed on the slab, E_{mol} is the energy of the isolated molecule, and E_{slab} is the energy of the clean slab surface. The calculation content is shown in Table S1.

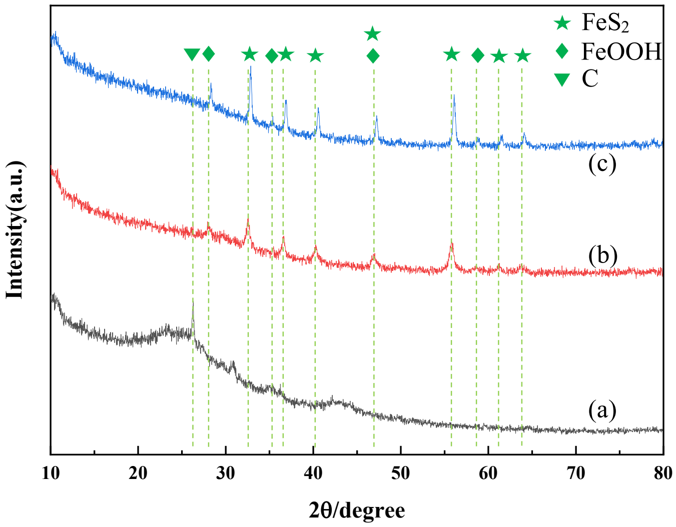

Fig. 1: XRD patterns of activated carbon (a), pyrite (b), and FeS_2@AC (c) after ball milling.

3. Results and discussion

3.1 Composite material characterization

Fig. 1 displays the X-ray diffraction (XRD) patterns of ball-milled samples of activated carbon (a), pyrite (b), and FeS_2@AC (c). It is evident from the figure that a significant characteristic diffraction peak of C atoms exists at 26.3° for activated carbon (Fig. 1a), while pyrite exhibits characteristic diffraction peaks of cubic FeS_2 at 32.6°, 36.6°, 40.7°, 47.2°, 56.2°, 61.6°, and 64.1°, corresponding to (200), (210), (211), (220), (311), (321), and (131) crystal planes (Fig. 1b), respectively (JCPDS Card No. 71-0053).[44] The ball-milled sample FeS_2@AC not only shows all the diffraction peaks of cubic FeS_2, but also shows some distinct diffraction peaks at 27.9°, 35.4°, 47.2°, and 58.8° correspond well with the crystal planes (120), (111), (240), and (160) of FeOOH (JCPDS Card No. 29-0713) (Fig. 1c), indicating the formation of FeOOH during ball milling.[45] It can also be seen that the diffraction

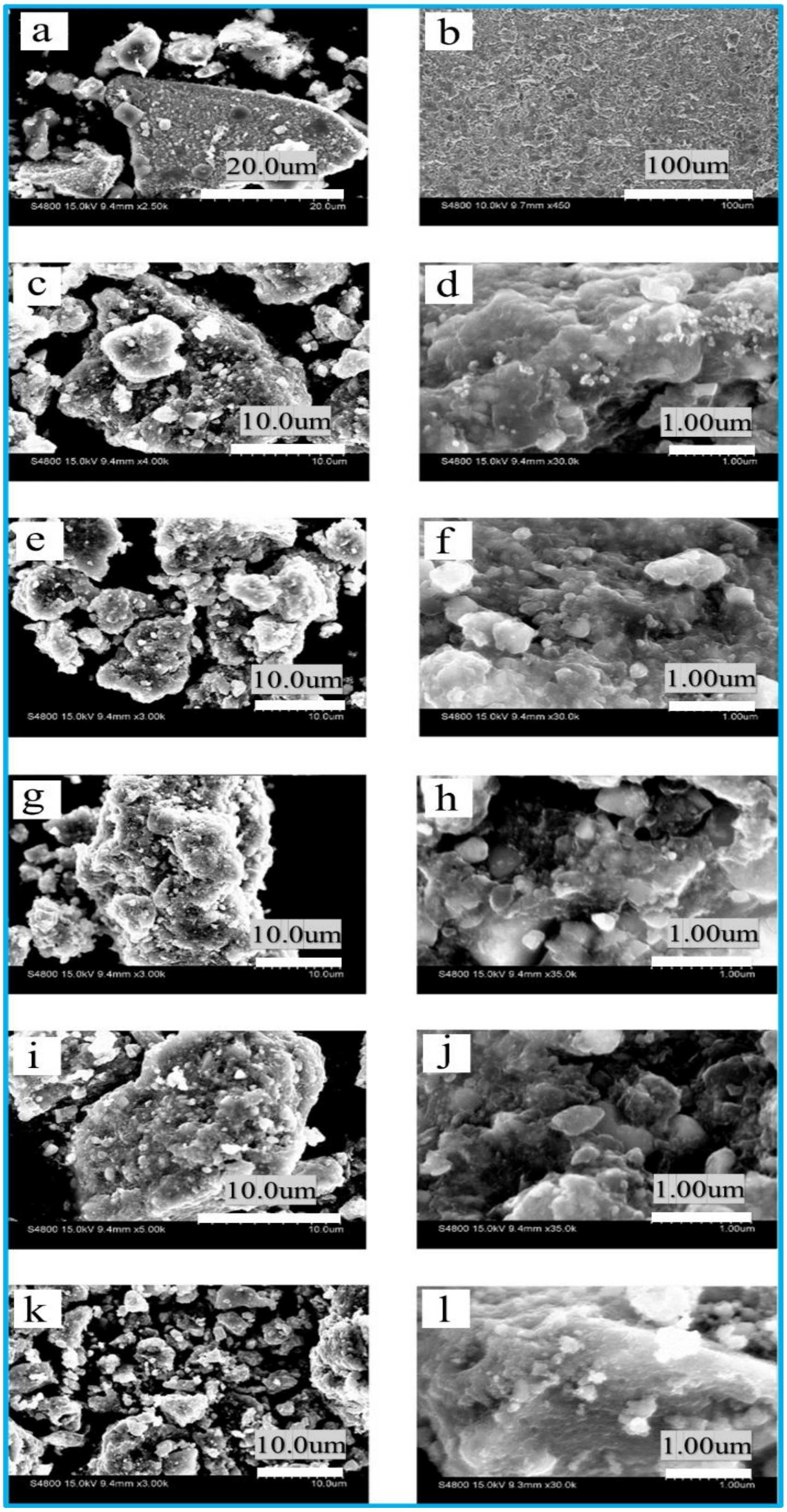

Fig. 2: SEM image of FeS_2 (a), AC (b), FeS_2@AC prepared by grinding for 3 h (c, d), 4h (e, f), 5h (g, h), 6h (i, j) and 7 h (k, l).

peak of FeS_2 in sample FeS_2@AC has a slight shift compared to sample FeS_2, which may be due to the interaction with activated carbon. Although nitrogen was initially introduced into the ball mill jar for protection, the particles were in large size before ball milling, and residual air may still exist in the gaps between the particles. During the ball milling process, the strong collision and friction between the grinding ball and the material will generate a large amount of heat, which may accelerate the oxidation reaction between FeS_2 with trace amounts of oxygen remaining in the tank.[46] In addition, the

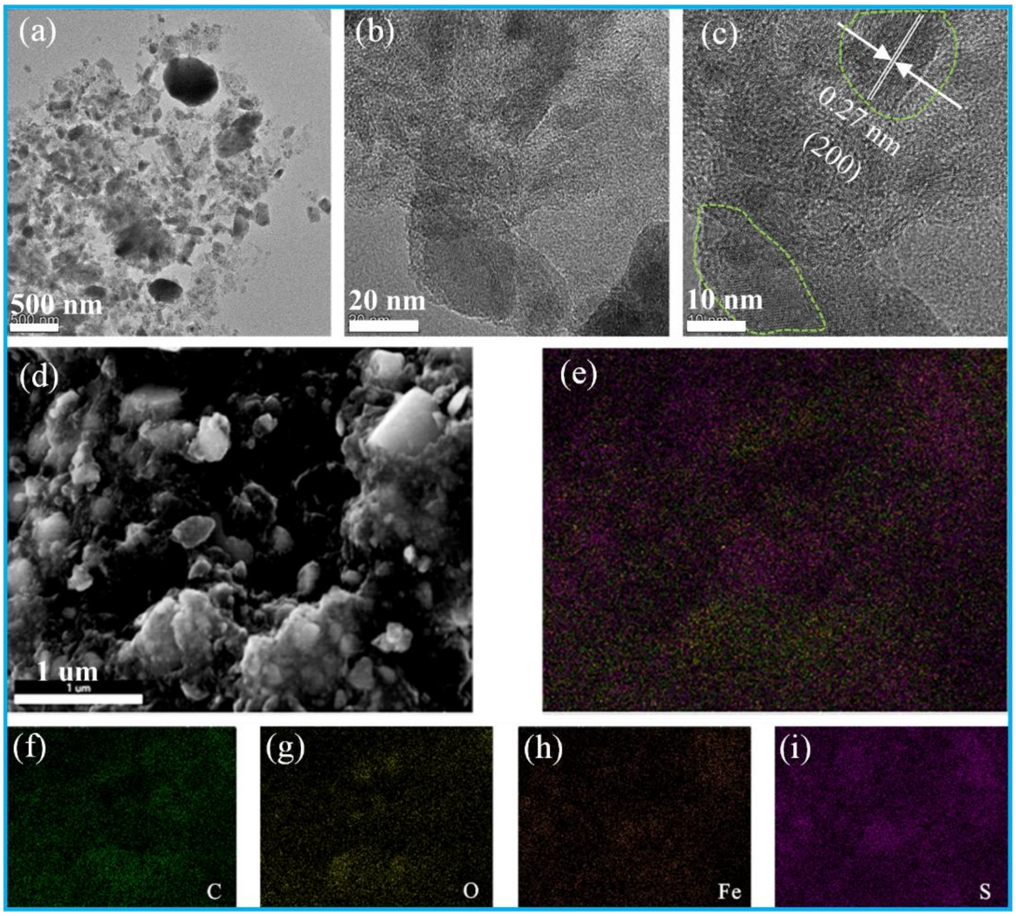

Fig. 3: TEM of FeS_2@AC (a-c), EDS diagram of FeS_2@AC (d-i).

functional groups on the surface of activated carbon can catalyze the reaction between FeS_2 and trace amounts of oxygen during ball milling, producing trivalent iron and hydroxylated iron oxide, especially under high-energy conditions such as ball milling.

Fig. 2 presents the SEM images of different samples before and after ball milling. Prior to ball milling, both pyrite and activated carbon exhibited a substantial, well-defined, three-dimensional structure. During the ball milling process, the materials experienced a variety of mechanical forces, including friction, collision, compression, grinding, shear, impact and extension.[47] These forces resulted in fracture, welding and deformation of the materials. Following this series of mechanical forces, the FeS_2@AC composites synthesized by ball milling underwent a significant change in morphology, transforming into smaller, irregularly shaped granular objects, as shown in the SEM of FeS_2@AC after milling for 3 h and 4 h. A portion of finer particles, presumably pyrite, were observed on the surface of these particles, suggesting potential loading on the surface and within the activated carbon. As the ball milling time increased, the originally larger pyrite and activated carbon particles gradually transformed into particulate matter with smaller particle sizes. However, with further increase in ball milling time to 5 h, a process of agglomeration becomes evident, resulting in some of the particulate matter increasing in size again. As shown in the SEM image, continue grinding for 7 h, the agglomerated particles will once again turn into fine particles, indicating that the grinding process is accompanied by complex physical and chemical changes. The presence of small particles on the surface of the activated carbon is clearly discernible, which are likely to be crystal FeS_2 formed during ball milling.

Figs. 3a-c show the TEM image of the sample FeS_2@AC. As shown in Fig. 3a, the overall ground sample presents a regular ellipsoid shape. The long diameter is 200 nm and the short diameter is 100 nm. Fig. 3b is the TEM image of nanoparticles with a size of approximately 20 nm that form the ellipsoidal shape. The lattice stripes in the dashed box of Fig. 3c indicate the crystallization of products during the ball milling process. The lattice stripe spacing is 0.27 nm, corresponding to the (200) crystal plane of FeS_2.[48] As shown in the energy spectrum analysis (EDS) results of FeS_2@AC presented in Figs. 3d-i, uniform distribution of C, O, Fe, and S elements was found, indicating that various substances have been uniformly dispersed in the obtained sample after grinding, which is beneficial for ensuring the stability of various properties of the sample during use. As shown in the Zeta potential test (Fig. S1), when the pH range is 2.6-4.8, FeS_2 carries a positive charge, while AC carries a negative charge. The pH during work is 3, and electrostatic attraction tightly connects the two.

Table 1: Orthogonal experimental design and its experimental results.

Orthogonal experiment	Ball milling conditions			Activation condition			Degradation rate (%)
	time (h)	Ball-material ratio	speed (rpm)	time (h)	FeS_2@AC dose (g/L)	PS conc. (mM)	
1	3	60	450	20	0.10	1	17.64
2	3	70	550	40	0.15	2	62.20
3	3	80	650	60	0.20	3	78.42
4	4	70	650	20	0.10	2	30.03
5	4	80	450	40	0.15	3	78.37
6	4	60	550	60	0.20	1	82.83
7	5	80	550	20	0.15	1	35.32
8	5	60	650	40	0.20	2	64.29
9	5	70	450	60	0.10	3	70.28
10	3	70	550	20	0.20	3	37.72
11	3	80	650	40	0.10	1	52.69
12	3	60	450	60	0.15	2	58.63
13	4	60	650	20	0.15	3	53.30
14	4	70	450	40	0.20	1	72.21
15	4	80	550	60	0.10	2	85.30
16	5	80	450	20	0.20	2	24.68
17	5	60	550	40	0.10	3	56.61
18	5	70	650	60	0.15	1	70.23

Table 2: Results of polar analysis of orthogonal experiments.

Level	Ball milling conditions			Activation condition		
	time (h)	Ball-material ratio	speed (rpm)	time (h)	FeS_2@AC dose (g/L)	PS conc. (mM)
1	51.1	55.6	53.6	63.8	33.0	52.1
2	67.0	57.0	59.9	74.9	64.4	59.7
3	53.6	59.1	58.2	82.4	74.3	59.9
Range %	15.9	3.5	6.3	41.3	7.8	8.2

3.2 Orthogonal experiments for degradation of tetracycline

Orthogonal experiments were designed for the degradation of tetracycline hydrochloride at concentrations of 50 mg/L and 100 mg/L by FeS_2@AC activated PS, respectively. The design of the orthogonal experiments for the degradation of tetracycline hydrochloride at 50 mg/L, along with the results thereof, is presented in Table 1. The analysis of the orthogonal experiments was conducted using polar analysis of variance and analysis of variance, as illustrated in Tables 2 and 3, respectively.

A comprehensive analysis of the experimental findings reveals that the activation time is the primary factor influencing the efficiency of tetracycline hydrochloride degradation, while the ball material ratio exhibits the least impact. Consequently, it can be deduced that the primary sequence of factors influencing the degradation efficiency is as follows: Activation time > Ball milling time > PS concentration > FeS_2@AC concentration > Ball milling speed > Ball material ratio. This conclusion is consistent with the results of the inverse analysis. The optimal process conditions for the preparation of FeS_2@AC and activation of PS for the degradation of 50 mg/L tetracycline hydrochloride were determined as follows: in the experiments conducted at a temperature of 25 °C, the ball milling duration was set at 4 h, with a ball-to-material ratio maintained at 80:1 and a ball

Table 3: The result of variance analysis for orthogonal experimental design.

Element	Sum of squared errors	Degrees of freedom	F-ratio	F critical value
Ball milling time	0.088	2	0.744	3.890
Ball material ratio	0.004	2	0.034	3.890
Ball milling speed	0.013	2	0.110	3.890
Activation time	0.557	2	4.704	3.890
FeS_2@AC concentration	0.024	2	0.203	3.890
PS concentration	0.024	2	0.203	3.890
Inaccuracies	0.710	12	--	--

Table 4: Orthogonal experimental design and its experimental results.

Orthogonal experiment	Ball milling conditions			Activation condition			Degradation rate (%)
	time (h)	Ball-mater. ratio	speed (rpm)	time (h)	FeS_2@AC dose (g/L)	PS conc. (mM)	
1	3	60	450	20	0.1	1	28.10
2	3	70	500	40	0.2	2	49.46
3	3	80	550	60	0.3	3	67.70
4	3	90	600	80	0.4	4	73.70
5	3	100	650	100	0.5	5	76.75
6	4	90	650	20	0.2	3	60.80
7	4	100	450	40	0.3	4	70.99
8	4	60	500	60	0.4	5	84.20
9	4	70	550	80	0.5	1	76.19
10	4	80	600	100	0.1	2	79.01
11	5	70	600	20	0.3	5	53.66
12	5	80	650	40	0.4	1	52.98
13	5	90	450	60	0.5	2	66.68
14	5	100	500	80	0.1	3	61.10
15	5	60	550	100	0.2	4	68.33
16	6	10	550	20	0.4	2	45.60
17	6	60	600	40	0.5	3	50.98
18	6	70	650	60	0.1	4	59.80
19	6	80	450	80	0.2	5	68.83
20	6	90	550	100	0.3	1	56.00
21	7	80	500	20	0.5	4	47.20
22	7	90	550	40	0.1	5	45.12
23	7	100	600	60	0.2	1	38.27
24	7	60	650	80	0.3	2	58.83
25	7	70	450	100	0.4	3	62.70

milling speed of 550 rpm. The activation time was optimized to 60 min, while the concentration of FeS_2@AC was adjusted to 0.3 g/L. The concentration of sodium persulfate was set at 2 mM, and the initial pH value of the solution was controlled at 3. Through practical experimental validation, we obtained the optimal degradation efficiency, achieving a degradation rate as high as 87.28%.

The configuration of the orthogonal experiment, with 100 mg/L tetracycline hydrochloride as the degradation target, is delineated in Table 4. The analysis of the orthogonal experiment was conducted through polar analysis of variance and analysis of variance to ascertain the pertinent outcomes, as illustrated in Tables 5 and 6.

Considering the experimental findings, it was determined that among the factors influencing the degradation efficiency of tetracycline hydrochloride, the activation time exhibited the most significant polar deviation, while the ball milling speed demonstrated the least polar deviation. Consequently, it can be deduced that the order of precedence of the influence of the factors on the degradation efficiency is: Activation time > Ball milling time > PS concentration > FeS_2@AC concentration > Ball material ratio > Ball milling speed. This conclusion was corroborated by inverse analysis. The process conditions were optimized for the preparation of FeS_2@AC and activation of PS for the degradation of 100 mg/L tetracycline hydrochloride by ball milling of iron ore composite activated carbon. The optimal conditions that were established for this process are outlined below: the temperature was maintained at 25 °C, the ball milling time was set at 4 h, the ball feed ratio was used at 80:1, the ball milling speed was set at 550 r/min, the activation time was extended to 100 min, and the concentration of FeS_2@AC was adjusted to 0.4 g/L, the concentration of sodium persulfate was elevated to 5 mM, and the initial pH value of the solution was maintained at 3. Performing the experiments under these conditions, the optimal degradation rate of 85.62% was obtained. Comparative summary of TC degradation at 50 mg/L and 100 mg/L under different conditions is shown in Table S2.

3.3 Mechanistic analysis

FeS_2@AC composites at a concentration of 0.1 g/L were co-located with 1 mM sodium persulfate in 50 mg/L tetracycline hydrochloride solution, and the reaction was allowed to continue for 1 h. Subsequently, the remaining solid powders were separated by filtration and placed in a vacuum drying oven at 80 °C for 1 h. Following the conclusion of the drying process, the samples were sealed. The elemental valence changes of FeS_2@AC activated persulfate (PS) during the degradation of tetracycline hydrochloride were investigated by means of comparative analyses using X-ray photoelectron spectroscopy (XPS) technique. As illustrated in Fig. 4a, the XPS full spectrogram of the FeS_2@AC composite clearly indicates the presence of Fe, O, C and S atoms. A comparison of the Fig. 4b plot with the FeS_2@AC composite reveals a significant weakening of the characteristic peaks of the O atoms. This phenomenon can be attributed to the reaction of the S atoms with the PS (persulfate) to form SO_4^{2-}, and these sulfate ions were subsequently dissolved in the tetracycline hydrochloride solution.[49] Figs. 4c, d reveal that the concentrations of Fe^{2+} and Fe^{3+} ions in the solution remained relatively constant before and after activation.[50,51] Specifically, the percentage of Fe^{2+} decreased marginally from 57.88% to

Table 5: Results of polar analysis of orthogonal experiments.

Level	Ball milling conditions			Activation condition		
	time (h)	Ball-mater. ratio	speed (rpm)	time (h)	FeS_2@AC dose (g/L)	PS conc. (mM)
1	59.7	58.1	59.5	47.1	54.6	50.3
2	74.2	60.4	60.5	53.9	57.1	59.9
3	60.5	63.1	59.8	63.3	61.4	60.6
4	56.2	60.5	59.1	67.7	63.8	64.0
5	50.4	58.5	61.8	68.6	63.6	65.7
Range %	23.8	5.0	2.7	24.5	9.2	15.4

Table 6: The result of variance analysis for orthogonal experimental design.

Element	Sum of squared errors	Degrees of freedom	F-ratio	F critical value
Ball milling time	0.155	4	2.009	2.780
Ball material ratio	0.008	4	0.108	2.780
Ball milling speed	0.002	4	0.027	2.780
Activation time	0.174	4	2.357	2.780
FeS_2@AC conc.	0.033	4	0.447	2.780
PS conc.	0.071	4	0.962	2.780
Inaccuracies	0.210	24	--	--

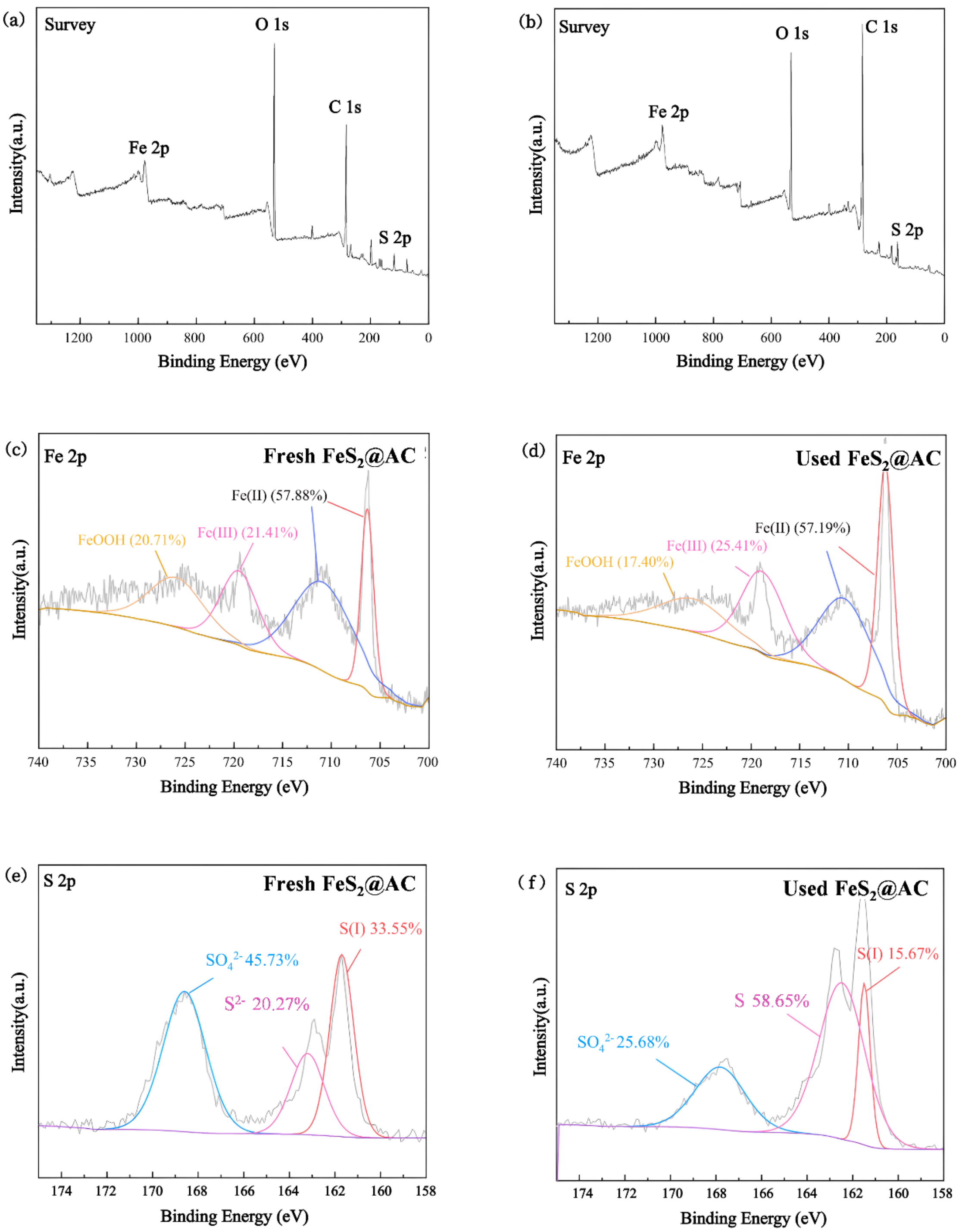

Fig. 4: XPS spectra of FeS$_2$@AC: (a) Pre-use full spectrum; (b) Post-use full spectrum; (c) Pre-use Fe 2p map; (d) Post-use Fe 2p map; (e) Pre-use S 2p map; (f) Post-use S 2p map.

57.19%, while the percentage of Fe^{3+} increased from 21.41% to 25.41%. Fig. 4e shows the presence of S^{-}, S^{2-} and SO$_4^{2-}$ of the fresh FeS$_2$.[52,53] Ball milling causes FeS$_2$ to decompose into FeS and S, which is further oxidized by O$_2$ to SO$_2$ and SO$_3$, ultimately generating SO$_4^{2-}$. Combining the analysis of plots Figs. 4e and 4f, it was found that the atomic content of S^{-} decreased significantly from 33.55% to 15.67%, while the S^{2-} peak at 163.2 eV changed into S^{0} peak at 162.5 eV, with peak area increased from 20.27% to 58.65%. This observation suggests that during the activation process, a portion of Fe^{2+} is involved in the activation of PS and converted to Fe^{3+}, while S^{-} may reduce part of Fe^{3+} back to Fe^{2+} under a certain mechanism as shown in Eq. (3).[54] Consequently, the overall change in the content of Fe^{2+} and Fe^{3+} ions is not significant. Furthermore, a decline in the content of SO$_4^{2-}$ from 45.73% to 25.68% was observed, presumably due to the dissolution of some SO$_4^{2-}$ in the tetracycline hydrochloride solution.

$$S^{-} + Fe^{3+} = S + Fe^{2+} \tag{3}$$

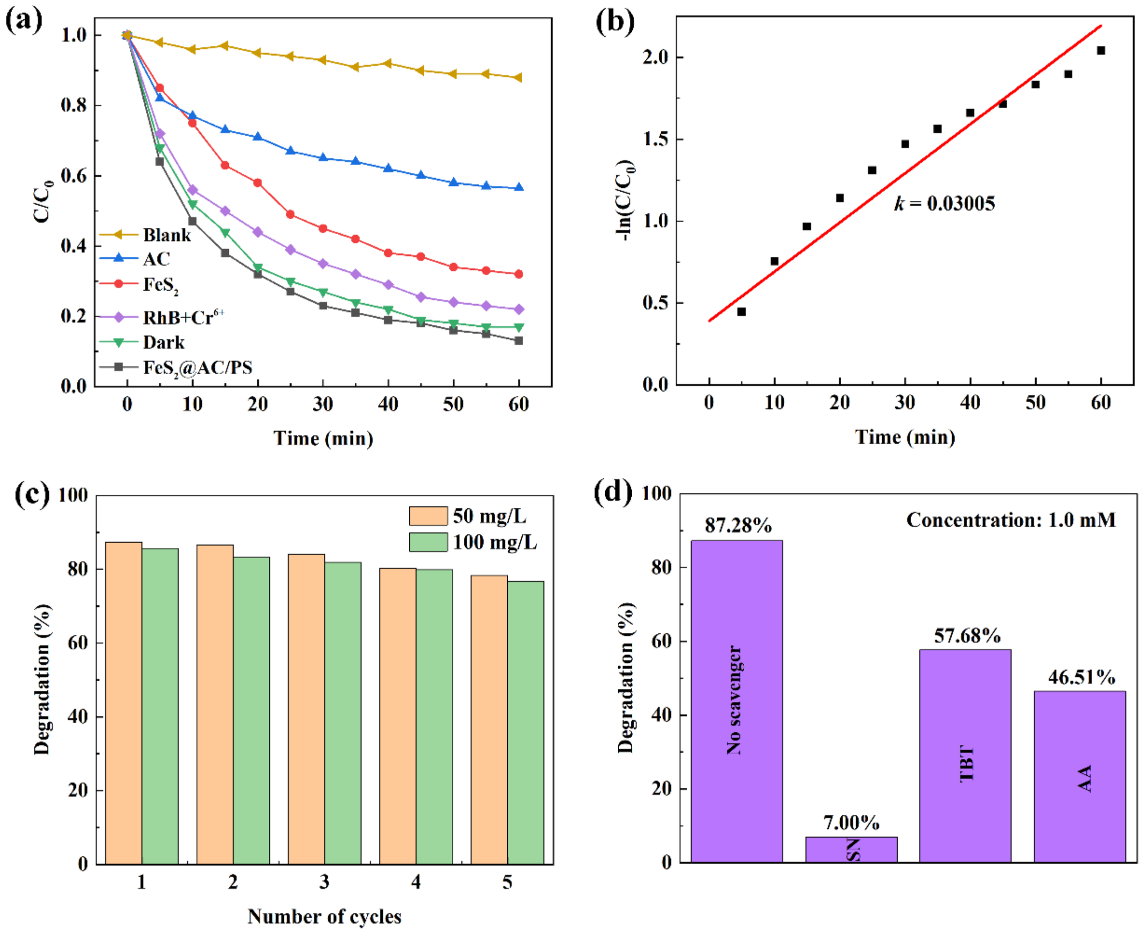

Fig. 5: (a) The degradation of TC over different samples; (b) Kinetic linear simulation curves for degradation of TC over FeS$_2$@AC; (c) Recyclability of FeS$_2$@AC for five times; (d) The degradation when using different quenching agents.

We conducted degradation experiments under different influencing factors to determine the role of sulfite activation. As shown in Fig. 5a, to avoid the effects of photolysis or photocatalysis, we conducted experiments of FeS$_2$@AC/PS system in dark, and the degradation curve of tetracycline was basically the same as that under natural light conditions; The blank tetracycline solution showed no degradation under natural light, and showed ~10% degradation under a 500 W xenon lamp after 1 h. This fully demonstrates that the degradation of tetracycline is caused by persulfate activation, rather than by photocatalysis or photolysis. The degradation efficiency of single component FeS$_2$ reaches 67.95%, while the removal rate of tetracycline by activated carbon is only 43.38%. In the presence of RhB (10 mg/L) and Cr^{6+} ions (10 mg/L), the degradation rate of TC is 78.19%, indicating that other pollutants have insignificant effect on the activation of persulfate for TC degradation. The degradation process is fit to pseudo-first-order kinetics, $-\ln(C/C_0) = kt$, where k is the reaction apparent rate constant and t is time, as shown in Fig. 5b. The constant speed is basically 0.03005, which is faster in the first 30 min and slightly slower in the last 30 min. At 30 min, the degradation rate had reached 76.94%, indicating the excellent effect of this technology. Fig. 5c shows that after 5 cycles, the degradation rates decreased from 87.12% and 85.53% to 78.36% and 76.69%, with loss rates were only 10.06% and 10.34%, respectively. The degradation rates of 50mg/L and 100mg/L tetracycline hydrochloride remained above 80% after 4 cycles, indicating the good stability of the activator. The free radical quenching experiment showed that the degradation rate was 87.28% without the addition of quenching agent. After adding 1.0mM sodium nitrite (SN), tert butanol (TBT), and ascorbic acid (AA), the degradation rates of TC were 7.00%, 57.68%, and 46.51%, respectively. This indicates that the main free radicals are $SO_4^{-\bullet}$, followed by OH$^{\bullet}$ radicals. However, holes and superoxide ions have little effect (Fig.5d).

As demonstrated in Fig. S2a, the ESR spectrum of pure ammonium persulfate (concentration of 1 mM) is shown. A thorough analysis of this figure reveals that in the system of sodium persulfate solution alone, the production of reactive radicals is minimal, which rationally explains why the pure sodium persulfate system exhibits a very low rate in the degradation of tetracycline. In contrast, when FeS$_2$@AC powder (concentration of 0.1 g/L) was added to the system

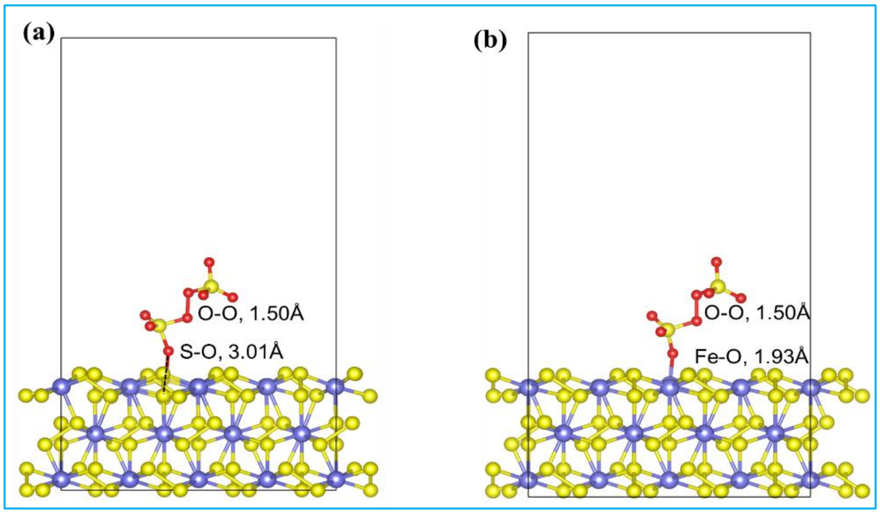

Fig. 6: Molecular configuration of PS adsorption on the S sites (a) and Fe sites (b) of the FeS_2.

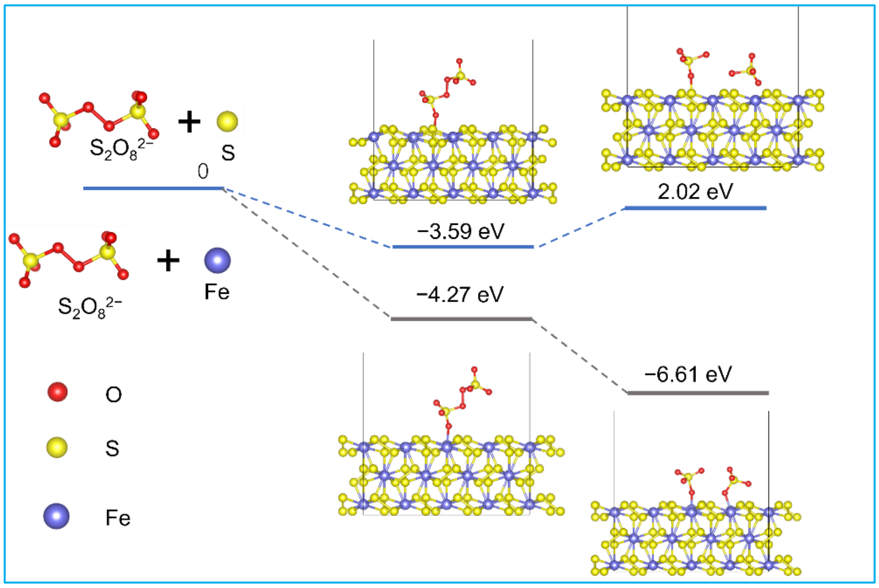

Fig. 7: DFT-derived energy step diagram for FeS_2-activated persulfate conversion to sulfate radicals, illustrating adsorption and activation energy changes on iron and sulfur interaction sites.

shown in Fig. S2b, characteristic peaks corresponding to hydroxyl radicals ($OH^{\bullet}$) and sulfate radicals ($SO_4^{-\bullet}$) became prominent in the FeS_2@AC/PS system, and these peaks were of comparable intensity.[55] It is noteworthy that $SO_4^{-\bullet}$ is produced by the activation of sodium persulfate by FeS_2@AC, whereas $OH^{\bullet}$ is mainly converted from $SO_4^{-\bullet}$ with hydroxide ions (OH^-) in water by some mechanism as shown in Eq. (4). This finding provides strong evidence that FeS_2@AC can activate sodium persulfate efficiently, which significantly promotes its decomposition and releases reactive free radicals.

$$SO_4^- \cdot + OH^- = SO_4^{2-} + \cdot OH \tag{4}$$

To elucidate more comprehensively the influence of sulfur (S) and iron (Fe) sites within pyrite on the activation of persulfate (PS, $S_2O_8^{2-}$), we employed density functional theory (DFT) calculations to model the adsorption and activation dynamics of PS on the (100) lattice plane of pyrite. Fig. 6 provides a visual representation of the adsorption bond lengths of $S_2O_8^{2-}$ at the S site and Fe site. The adsorption bond lengths at the S site and Fe site are shown. The Fe-O bond length is 1.93 Å, and the S-O bond length is 3.01 Å. Usually, the shorter the chemical bond, the stronger the interatomic force. It can be seen that the force of PS adsorption on Fe sites is stronger.

As demonstrated in Fig. 7, the reaction pathway of this experiment is simulated. The initial stage is representative of the unadsorbed state of $S_2O_8^{2-}$ and FeS_2, with an initial relative energy of 0. The subsequent stage is representative of the energy change when $S_2O_8^{2-}$ adsorbs onto the surface, with negative values indicating exothermic reactions. The upper and lower parts correspond to the S site and Fe site, respectively. As demonstrated by the Fig. 7, the adsorption energy of $S_2O_8^{2-}$ at the Fe site is lower (-4.27 eV vs -3.59 eV), indicating that Fe site is more favorable for adsorption. The third stage of the process represents the energy required for the formation of the $SO_4^{-\bullet}$ radical. From a topographical perspective, the formation of a radical at the S site necessitates the absorption of heat from the external environment. In contrast, the reaction at the Fe site is characterized as exothermic, thereby facilitating the formation of free radicals. Collectively, these findings indicate that Fe^{2+} plays a pivotal role in PS activation, while sulfur atoms in pyrite function as electron donors to facilitate the regeneration of Fe^{2+} from Fe^{3+} as described in Eq. (3), thereby sustaining the catalytic cycle.

The mechanism of activating persulfate to generate free radicals for the degradation of tetracycline is shown in Fig. 8. The enormous shear force during the mechanochemical ball milling process causes FeS_2 particles to become nano-sized, possessing high surface energy for PS activation. During the activation of persulfate by FeS_2@AC, sulfate radicals ($SO_4^{-\bullet}$) and hydroxyl radicals ($OH^{\bullet}$) are primarily generated, with sulfate radicals ($SO_4^{-\bullet}$) playing a significant role in the degradation process.[56] It is noteworthy that the sulfur atom (S^-) within the FeS_2@AC structure exhibits reductive properties, capable of reversing the electron configuration of Fe^{3+} to Fe^{2+}. This process is a continuous activation of PS, as illustrated in Fig. 8. Finally, under the attack of sulfate radicals ($SO_4^{-\bullet}$) and hydroxyl radicals ($OH^{\bullet}$), tetracycline is degraded into small molecules.

To investigate the intermediates formed in the photocatalytic decomposition of TC by FeS_2@AC, liquid chromatography-mass spectrometry (LC-MS) was used to analyze the constituents of the response mixture for various response times. Two plausible degradation pathways of TC (m/z = 445) are depicted in Fig. 9a. In Pathway 1, TC removes the functional group containing N and opens a benzene ring to form A1 (m/z = 453). Then, the outer branch is removed, and the benzene ring on the second outer side opens to form A2 (m/z = 365), followed by the formation of A3 (m/z = 141) in the same carbocycle cleavage reaction. In Pathway 2, TC loses a methyl group, yielding product B1 (m/z = 431), which remove one amide group and hydroxyl group to form B2 (m/z = 358). After carbocycle cleavage reaction, B2 changed into B3 (m/z = 208). Additionally, intermediates A3 and B3 are subject to attack by side chains and rings, leading to gradual decomposition into smaller molecules, including T1 (m/z = 143), T2 (m/z = 147), T3 (m/z = 115) and T4 (m/z = 74). These intermediates can be subsequently decomposed into smaller molecules such as CO_2 and H_2O.

The toxicity estimation software tool (T.E.S.T.) was adopted to evaluate the toxicity of TC and its' intermediate products. As shown in Fig. 9b, "Fathead minnow LC 50 (96 h)" is the concentration of a chemical substance that causes 50% of fat headed fish to die within 96 h. The smaller the value, the stronger the toxicity. The concentrations of the intermediates of A3 (26.79 mg/L), B32 (42.17 mg/L), T1 (244.00 mg/L), T2 (1720.21 mg/L), T3 (119.98 mg/L), and T4 (206.36 mg/L) were all higher than that of TC (0.90 mg/L), indicating that the intermediates have reduced toxicity. Bioconcentration Factor (BCF) is a key indicator used in toxicology to measure the ability of chemicals to accumulate in organisms. Fig. 9c indicates that the intermediates A1, A2, B1, T1, and T2 have a lower bioaccumulation potential compared to TC. In toxicology analysis, mutagenicity refers to the ability of chemical substances, physical factors, or biological factors to cause permanent changes in the genetic material of an organism, and the intermediates B3, T1, T2, T3 and T4 have reduced mutagenicity compared to TC, Fig. 9d. The developmental toxicity of intermediates A1 (0.67), A2 (0.78), A3 (0.71), B2 (0.77), B3 (0.68), T2 (0.73), T3 (0.74), and T4 (0.77) were also lower than that of TC (0.86). T1 with the value of 0.26 is developmental non-toxicant (Fig. 9e). In summary, while the initial degradation of TC may generate intermediates with higher toxicity, these compounds are ultimately transformed into less harmful products and completely mineralized into innocuous substances like CO_2 and H_2O.

This technology is easy to operate, suitable for mechanized operation, and reduces labor costs. The ball milling time is only 6 h, which is much shorter than the duration and energy

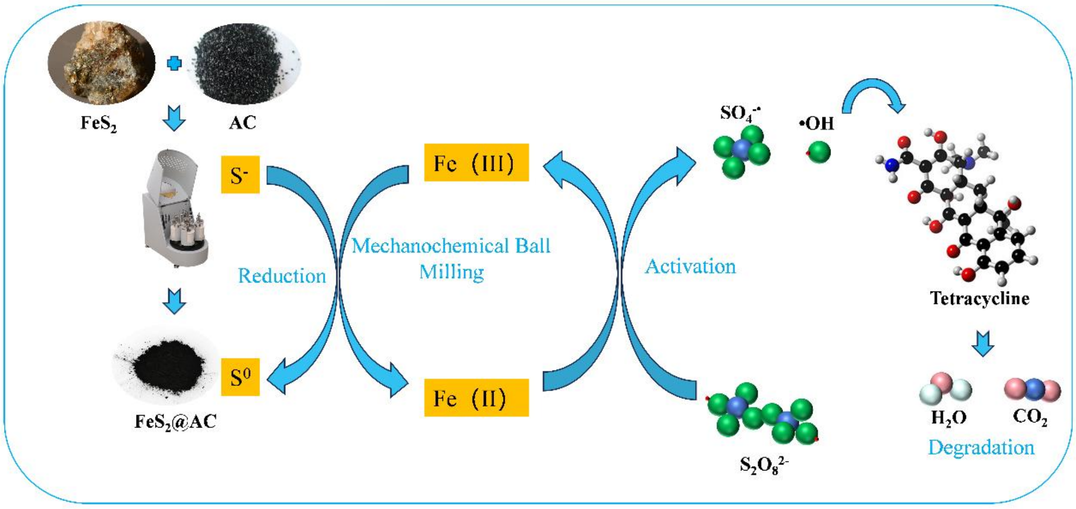

Fig. 8: Schematic diagram of persulfate activation by FeS_2@AC to generate sulfate radical and degrade TC.

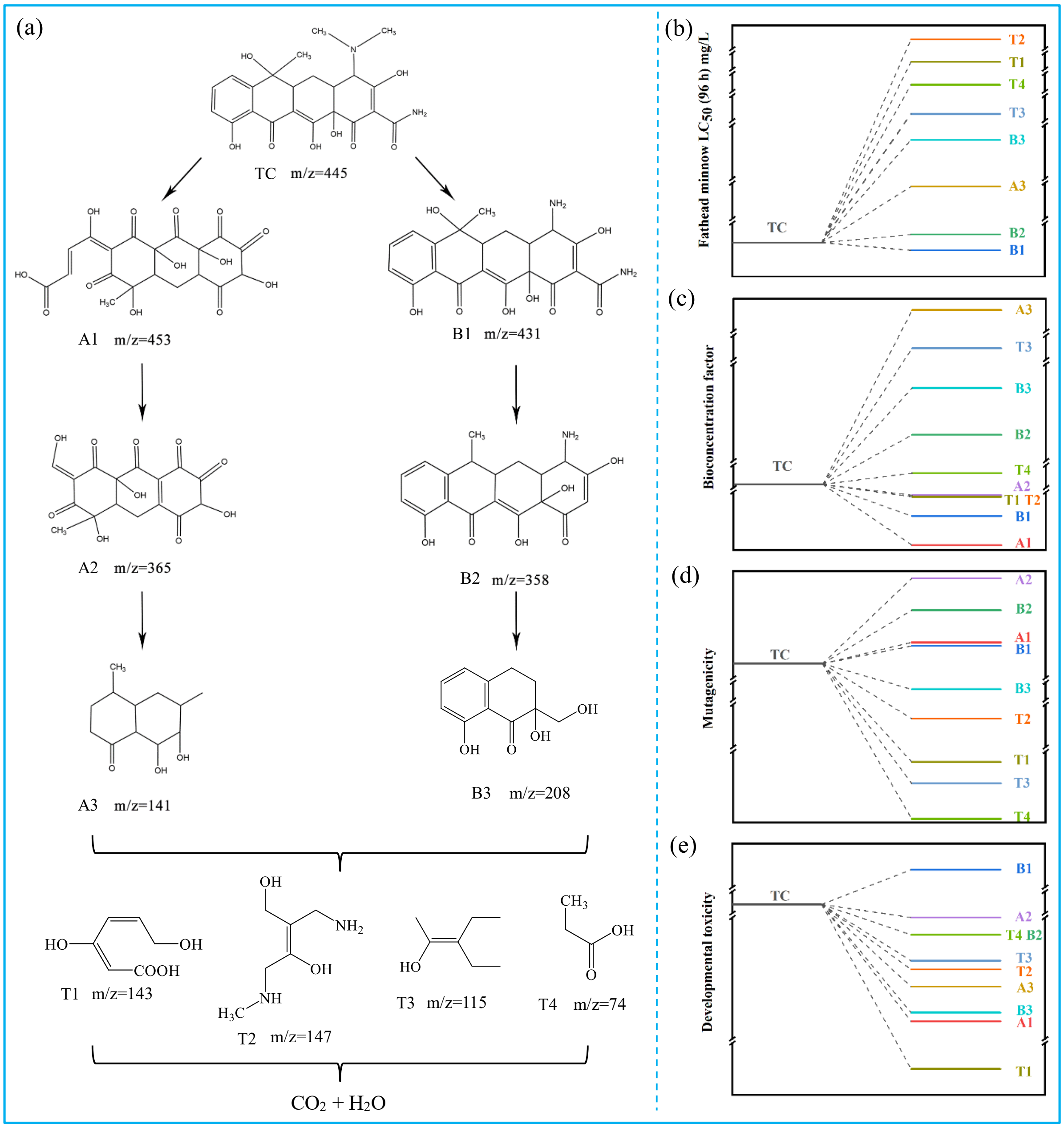

Fig. 9: (a) Possible path of tetracycline hydrochloride degradation. (b) Fathead minnow LC50 (96 h), (c) the bioconcentration factor, (d) mutagenicity and (e) developmental toxicity of TC and its intermediates.

consumption of the hydrothermal method.The cost of treating tetracycline per ton of water is approximately $11.8, and the next step is to use primary ore to further reduce the cost. For large-scale production, it is recommended to optimize the continuous ball milling process from two aspects: firstly, by adjusting the ball to material ratio, rotation speed, and nitrogen protection parameters, the oxidation of intermediate products can be reduced, while avoiding particle agglomeration caused by excessive grinding; The second is to develop a continuous flow reaction system that combines ball milling preparation with activated degradation processes to improve processing efficiency and further reduce the cost of large-scale applications.

4. Conclusion

This work successfully prepared FeS_2@AC nanoscale composites via mechanochemical ball milling of pyrite and activated carbon. The composites effectively activated persulfate (PS) to generate sulfate radicals ($SO_4^{-\bullet}$) and hydroxyl radicals (·OH), with $SO_4^{-\bullet}$ being the dominant species for tetracycline hydrochloride (TC) degradation. Orthogonal experiments were conducted to identify the optimal conditions, and the activation time were found to be the most important key factor. At concentrations of 50 mg/L and 100 mg/L of TC, degradation efficiencies of 87.28% and 85.62% were achieved, respectively. Experimental data and density functional theory (DFT) calculations indicate that Fe^{2+}

is the main catalytic site, and S$^-$ mainly promotes the cycling of Fe between different valence states during the reaction process, eliminating the necessity of adding any reducing agents. The degradation mechanism and the toxicity of the intermediates were also analyzed. This work provides insights into TC degradation intermediates and demonstrates feasible strategies for engineering environmental remediation. The limitation of this work is that the use of pure chemical reagents increased the cost. Next, we will investigate the activation ability of primary ores towards persulfate.

Acknowledgements

This work was financially supported by the Natural Science Foundation of China (Nos. 21806101, 52070127), Shanghai Shuguang Program (21SG55), Local Capacity Construction (22010500800), and 2022 Annual Project of the Chinese Society for Technical and Vocational Education-China Institute of Vocational Education in the New Era-Research on the Cultivation of Technical and Skilled Talents for the Double Carbon Strategy (No. SZ22B48).

Conflict of Interest

There is no conflict of interest.

Supporting Information

Applicable.

References

[1] Y. X. Pei, A. J. Lei, S. Yang, H. G. Chen, X. Y. Liu, L. W. Liu, X. T. Kang, Biodegradation and bioaugmentation of tetracycline by Providencia stuartii TX2: Performance, degradation pathway, genetic background, key enzymes, and application risk assessment, *Journal of Hazardous Materials*, 2024, **477**, 135231, doi: 10.1016/j.jhazmat.2024.135231.

[2] H. Zhang, J. M. Bian, C. G. Yang, Z. C. Hu, F. Y. Liu, C. P. Zhang, Removal of tetracycline from livestock wastewater by positive single pulse current electrocoagulation: Mechanism, toxicity assessment and cost evaluation, *Science of The Total Environment*, 2022, **810**, 151955, doi: 10.1016/j.scitotenv.2021.151955.

[3] Y. J. Dai, M. Liu, J. J. Li, S. S. Yang, Y. Sun, Q. Y. Sun, W. S. Wang, L. Lu, K. X. Zhang, J. Y. Xu, W. L. Zheng, Z. Y. Hu, Y. H. Yang, Y. W. Gao, Z. H. Liu, A review on pollution situation and treatment methods of tetracycline in groundwater, *Separation Science and Technology*, 2020, **55**, 1005-1021, doi: 10.1080/01496395.2019.1577445.

[4] A. K. Sarmah, M. T. Meyer, A. B. A. Boxall, A global perspective on the use, sales, exposure pathways, occurrence, fate and effects of veterinary TC (VAs) in the environment, *Chemosphere*, 2006, **65**, 725-759, doi: 10.1016/j.chemosphere.2006.03.026.

[5] A. Önal, Overview on liquid chromatographic analysis of tetracycline residues in food matrices, *Food Chemistry*, 2011, **127**, 197-203, doi: 10.1016/j.foodchem.2011.01.002.

[6] Z. F. Yu, Y. Yang, H. F. Zhuang, S. D. Shan, M. S. Beldean-Galea, Q. Q. Xue, X. F. Shen, S. J. Li, In-situ growth of MIL-53 (Fe) on charcoal sponge as a highly efficient and recyclable photocatalyst for removal of Cr(VI), *Rare Metals*, 2024, **43**, 4344-4355, doi: 10.1007/s12598-024-02725-6.

[7] J. L. Zhang, G. J. Yu, C. Y. Yang, S. J. Li, Recent progress on S-scheme heterojunction strategy enabling polymer carbon nitrides C_3N_4 and C_3N_5 enhanced photocatalysis in energy conversion and environmental remediation, *Current Opinion in Chemical Engineering*, 2024, **45**, 101040, doi: 10.1016/j.coche.2024.101040.

[8] S. M. Mousavi, M. S. Mohtaram, K. Rasouli, S. Mohtaram, H. Rajabi, S. Sabbaghi, Efficient visible-light-driven photocatalytic degradation of antibiotics in water by MXene-derived TiO_2-supported SiO_2/Ti_3C_2 composites: Optimisation, mechanism and toxicity evaluation, *Environmental Pollution*, 2025, **367**, 125624, doi: 10.1016/j.envpol.2024.125624.

[9] X. Y. Hu, G. Q. Xiao, C. L. Chen, C. Y. Chen, X. Zeng, R. L. Li, Z. W. Yang, Engineering Z-scheme $Bi_2S_3/CeO_2/Ni(OH)_2$ heterojunctions for enhanced visible-light photocatalytic degradation of tetracycline hydrochloride, *Catalysis Letters*, 2025, **155**, 172, doi: 10.1007/s10562-025-05003-x.

[10] S. Fekadu, E. Alemayehu, R. Dewil, B Van der Bruggen, Pharmaceuticals in freshwater aquatic environments: A comparison of the African and European challenge, *Science of the Total Environment*, 2019, **654**, 324-37, doi: 10.1016/j.scitotenv.2018.11.072.

[11] D. Cheng, H. H. Ngo, W. S. Guo, S. W. Chang, D. D. Nguyen, Y. W. Liu, Q. Wei, D. Wei, A critical review on antibiotics and hormones in swine wastewater: Water pollution problems and control approaches, *Journal of Hazardous Materials*, 2020, **387**, 121682, doi: 10.1016/j.jhazmat.2019.121682.

[12] J. Y. Cao, L. D. Lai, B. Lai, G. Yao, X. Chen, L. P. Song, Degradation of tetracycline by peroxymonosulfate activated with zero-valent iron: Performance, intermediates, toxicity and mechanism, *Chemical Engineering Journal*, 2019, **364**, 45-56, doi: 10.1016/j.cej.2019.01.113.

[13] D. J. Feng, X. Y. Li, Y. P. Liu, X. B. Chen, S. J. Li, Emerging Bismuth-Based Step-Scheme Heterojunction Photocatalysts for Energy and Environmental Applications, *Renewables*, 2023, **1**, 485–513, doi: 10.31635/renewables.023.202300037.

[14] C. Q. Zhuang, W. M. Li, Y. Chang, S. J. Li, Y. H. Zhang, Y. L. Li, J. F. Gao, G. Chen, Z. H. Kang, Coordination environment dominated catalytic selectivity of photocatalytic hydrogen and oxygen reduction over switchable gallium and nitrogen active sites, *Journal of Materials Chemistry A*, 2024, **12**, 5711-5718, doi: 10.1039/D3TA07951A.

[15] L. L. Yan, X. Song, J. W. Miao, Y. F. Ma, T. Zhao, M. Y. Yin, Removal of tetracycline from water by adsorption with biochar: A review, *Journal of Water Process Engineering*, 2024, **60**, 105215, doi: 10.1016/j.jwpe.2024.105215.

[16] B. S. Zakaria, B. R. Dhar, A Review of stand-alone and hybrid microbial electrochemical systems for TC removal from wastewater, *Processes* 2022, **10**, 714, doi: 10.3390/pr10040714.

[17] A. R. Huang, M. T. Yan, J. J. Lin, L. J. Xu, H. Gong, H. Gong, A review of processes for removing antibiotics from breeding

wastewater, *International Journal of Environmental Research and Public Health*, 2021, **18**, 4909, doi: 10.3390/ijerph18094909.

[18] J. N. Russell, C. K. Yost, Alternative, environmentally conscious approaches for removing antibiotics from wastewater treatment systems, *Chemosphere*, 2021, **263**, 128177, doi: 10.1016/j.chemosphere.2020.128177.

[19] A. Mukimin, H. Vistanty, N. Zen, Hybrid advanced oxidation process (HAOP) as highly efficient and powerful treatment for complete demineralization of antibiotics, *Separation and Purification Technology*, 2020, **241**, 116728, doi: 10.1016/j.seppur.2020.116728.

[20] N. Xing, Y. G. Zhang, Three-dimensional electrochemical treatment of tetracycline hydrochloride with transition metal-loaded carbon felts in combination with coagulation chemicals, *Journal of Environmental Chemical Engineering*, 2024, **12**, 114899, doi: 10.1016/j.jece.2024.114899.

[21] H. Zou, J. T. He, B. N. He, T. Y. Lao, F. Liu, X. Y. Guan, Sensitivity assessment of denitrifying bacteria against typical antibiotics in groundwater, *Environmental Science-Processes & Impacts*, 2019, **21**, 1570-1579, doi: 10.1039/c9em00275h.

[22] S. Y. Zuo, D. Y. Li, H. M. Xu, D. S. Xia, An integrated microwave-ultraviolet catalysis process of four peroxides for wastewater treatment: Free radical generation rate and mechanism, *Chemical Engineering Journal*, 2020, **380**, 122434, doi: 10.1016/j.cej.2019.122434.

[23] C. Le, J. H. Wu, P. Li, X. D. Wang, N. W. Zhu, P. X. Wu, B. Yang, Decolorization of anthraquinone dye Reactive Blue 19 by the combination of persulfate and zero-valent iron, *Water Science and Technology*, 2011, **64**, 754-759, doi: 10.2166/wst.2011.708.

[24] Y. T. Zeng, H. Qiu, J. Zeng, Y. Gao, Z. X. Ding, Z. Q. Xie, C. Y. Wang, Degradation of beneficiation reagent ester-105 by light, heat, and microwave activated persulfate, *Water Air and Soil Pollution*, 2024, **235**, 98, doi: 10.1007/s11270-024-06906-y.

[25] J. H. Fan, Y. Cai, S. H. Shen, L. Gu, New insights into FeS/persulfate system for tetracycline elimination: Iron valence, homogeneous-heterogeneous reactions and degradation pathways, *Journal of Environmental Sciences*, 2022, **112**, 48-58, doi: 10.1016/j.jes.2021.04.031.

[26] H. Milh, J. Pessemier, D. Cabooter, R. Dewil, Removal of sulfamethoxazole by ferrous iron activation of persulfate: Optimization of dosing strategy and degradation mechanism. *Science of the Total Environment*, 2021, **799**, 149159, doi: 10.1016/j.scitotenv.2021.149159.

[27] T. Liu, K. Wu, M. Wang, C. Y. Jing, Y. Y. Chen, S. J. Yang, P. K. Jin, Performance and mechanisms of sulfadiazine removal using persulfate activated by Fe_3O_4@CuO_x hollow spheres, *Chemosphere*, 2021, **262**, 127845, doi: 10.1016/j.chemosphere.2020.127845.

[28] Q. L Ma, H. X. Zhang, X. Y. Zhang, B. Li, R. N. Guo, Q. F. Cheng, X. W. Cheng, Synthesis of magnetic $CuO/MnFe_2O_4$ nanocompisite and its high activity for degradation of levofloxacin by activation of persulfate, *Chemical Engineering Journal*, 2019, **360**, 848-60, doi: 10.1016/j.cej.2018.12.036.

[29] H. X. Zhang, Y. Y. Song, L. C. Nengzi, J. F. Gou, B. Li, X. W. Cheng, Activation of persulfate by a novel magnetic $CuFe_2O_4/Bi_2O_3$ composite for lomefloxacin degradation, *Chemical Engineering Journal*, 2020, **379**, 122362, doi: 10.1016/j.cej.2019.122362.

[30] Y. F. Du, M. Dai, I. Naz, X. Y. Hao, X. X. Wei, R. Rong, C. S. Peng, I. Ali, Carbothermal reduction synthesis of zero-valent iron and its application as a persulfate activator for ciprofloxacin degradation, *Separation and Purification Technology*, 2021, **275**, 119201, doi: 10.1016/j.seppur.2021.119201.

[31] M. F Cui, Y. H. Li, Y. Sun, H. M. Wang, M. X. Li, L. B. Li, W. S. Xu, Degradation of tetracycline in polluted wastewater by persulfate over copper alginate/graphene oxide composites, *Journal of Polymers and the Environment*, 2021, **29**, 2227-2235, doi: 10.1007/s10924-020-02038-6.

[32] X. X. Wu, T. Li, R. Z. Wang, Y. X. Zhang, W. Z. Liu, L. J. Yuan, One-pot green synthesis of zero-valent iron particles supported on N-doped porous carbon for efficient removal of organic pollutants via persulfate activation: Low iron leaching and degradation mechanism, *Separation and Purification Technology*, 2021, **279**, 119768, doi: 10.1016/j.seppur.2021.119768.

[33] F. Yin, C. Wang, K. Y. A. Lin, S. P. Tong, Persulfate activation for efficient degradation of norfloxacin by a rGO-Fe_3O_4 composite, *Journal of the Taiwan Institute of Chemical Engineers*, 2019, **102**, 163-169, doi: 10.1016/j.jtice.2019.05.022.

[34] J. Lee, M. Kim, S. Kim, Y. Ahn, B. Lee, D. Lee, Facile recycling of cemented tungsten carbide soft scrap via mechanochemical ball milling, *International Journal of Refractory Metals and Hard Materials*, 2021, **100**, 105645, doi: 10.1016/j.ijrmhm.2021.105645.

[35] N. J. Welham, T. Kerr, P. E. Willis, Ambient-temperature mechanochemical formation of titanium nitride-alumina composites from TiO_2 and $FeTiO_3$, *Journal of the American Ceramic Society*, 1999, **82**, 2332-2336, doi: 10.1111/j.1151-2916.1999.tb02087.x.

[36] B. Wang, B. Gao, Y. Wan, Entrapment of ball-milled biochar in Ca-alginate beads for the removal of aqueous Cd (II), *Journal of Industrial and Engineering Chemistry*, 2018, **61**, 161-168, doi: 10.1016/j.jiec.2017.12.013.

[37] X. G. Liu, Y. J. Li, L. Zeng, X. Li, N. Chen, S. B. Bai, H. N. He, Q. Wang, C. H. Zhang, A review on mechanochemistry: Approaching advanced energy materials with greener force, *Advanced Materials*, 2022, **34**, 2108327, doi: 10.1002/adma.202108327.

[38] P. F. M. de Oliveira, R. M. Torresi, F. Emmerling, P. H. C. Camargo, Challenges and opportunities in the bottom-up mechanochemical synthesis of noble metal nanoparticles, *Journal of Materials Chemistry A*, 2020, **8**, 16114-16141, doi: 10.1039/d0ta05183g.

[39] C. J. Huang, J. L. Hu, S. Cong, Z. G. Zhao, X. Q. Qiu, Hierarchical BiOCl microflowers with improved visible-light-driven photocatalytic activity by Fe (III) modification, *Applied Catalysis B: Environmental*, 2015, **174**, 105-112, doi: 10.1016/j.apcatb.2015.03.001.

[40] I. N. A. Al-Duais, S. Ahmad, M. M. Al-Osta, M. Maslehuddin, T. A. Saleh, S. U. Al-Dulaijan, Optimization of

alkali-activated binders using natural minerals and industrial waste materials as precursor materials, *Journal of Building Engineering*, 2023, **69**, 106230, doi: 10.1016/j.jobe.2023.106230.

[41] G. Kresse, J. Furthmüller, Efficient iterative schemes for ab initio total-energy calculations using a plane-wave basis set, *Physical Review B*, 1996, **54**, 11169-11186.

[42] J. P. Perdew, K. Burke, M. Ernzerhof, Generalized gradient approximation made simple. *Physical Review Letters*, 1996, **77**, 3865-3868.

[43] S. Grimme, J. Antony, S. Ehrlich, H. Krieg, A consistent and accurate ab initio parametrization of density functional dispersion correction (DFT-D) for the 94 elements H–Pu. *Journal of Chemical Physics*, 2010, **132**, 154104.

[44] X. Y. He, X. B. Min, T. Y. Peng, F. P. Zhao, Y. Ke, Y. Y. Wang, G. H. Jiang, Q. J. Xu, J. W. Wang, Mechanochemically activated microsized zero-valent iron/pyrite composite for effective hexavalent chromium sequestration in aqueous solution, *Journal of Chemical & Engineering Data*, 2020, **65**, 1936-1945, doi: 10.1021/acs.jced.9b01110.

[45] Q. Q. Xue, B. T. Song, Q. Feng, Z. F. Yu, K. W. Hu, Y. Yang, X. F. Shen, Efficiently removal of tetracycline via synergistic photocatalysis with Fenton reaction with biochar/FeOOH, *Applied Surface Science*, 2024, **645**, 158869, doi: 10.1016/j.apsusc.2023.158869.

[46] J. C. Tang, B. B. Zhao, H. H. Lyu, D. Li, Development of a novel pyrite/biochar composite (BM-FeS_2@BC) by ball milling for aqueous Cr(VI) removal and its mechanisms, *Journal of Hazardous Materials*, 2021, **413**, 125415, doi: 10.1016/j.jhazmat.2021.125415.

[47] Z. F. Zhao, X. M. Jiang, Z. W. Dai, X. L. Li, J. Y. Peng, J. Zhong, F. Zhou, Experimental study and numerical simulation of the influence of ball milling on mechanical and physical properties of matcha powder, *Powder Technology*, 2024, **433**, 119213, doi: 10.1016/j.powtec.2023.119213.

[48] L. L. Ma, X. M. Zhou, J. Sun, P. Zhang, B. X. Hou, S. H. Zhang, N. Z. Shang, J. J. Song, H. J. Ye, H. Shao, Y. F. Tang, X. X. Zhao, Synergy mechanism of defect engineering in $MoS_2/FeS_2/C$ heterostructure for high-performance sodium-ion battery, *Journal of Energy Chemistry*, 2023, **82**, 268-276, doi: 10.1016/j.jechem.2023.03.011.

[49] M. M. Ye, Y. Q. Yan, W. Jin, X. Y. Wang, X. H. Zhou, T. Q. Zhang, X. W. Liu, Synergistic activation of peroxydisulfate by photothermal and FeS_2-loaded air-laid cloth in a shallow continuous flow reactor, *Journal of Hazardous Materials*, 2025, **487**, 137227, doi: 10.1016/j.jhazmat.2025.137227.

[50] S. J. Li, C. C. Wang, K. X. Dong, P. Zhang, X. B. Chen, X. Li, MIL-101(Fe)/BiOBr S-scheme photocatalyst for promoting photocatalytic abatement of Cr(VI) and enrofloxacin antibiotic: Performance and mechanism, *Chinese Journal of Catalysis*, 2023, **51**, 101-112, doi: 10.1016/S1872-2067(23)64479-1.

[51] C. C. Wang, C. J. You, K. Rong, C. Q. Shen, F. Yang, S. J. Li, An S-Scheme MIL-101(Fe)-on-BiOCl Heterostructure with Oxygen Vacancies for Boosting Photocatalytic Removal of Cr(VI), *Acta Physico-Chimica Sinica*, 2024, **40**, 2307045, doi: 10.3866/PKU.WHXB202307045.

[52] S. J. Li, C. J. You, K. Rong, C. Q. Zhuang, X. B. Chen, B. Zhang, Chemically bonded $Mn_{0.5}Cd_{0.5}S$/BiOBr S-scheme photocatalyst with rich oxygen vacancies for improved photocatalytic decontamination performance, *Advanced Powder Materials*, 2024, **3**, 100183, doi: 10.1016/j.apmate.2024.100183.

[53] D. Y. Ma, Q. Q. Xue, Y. P. Liu, F. L. Liang, W. Y. Li, T. Liu, C. Q. Zhuang, Z. W. Zhao, S. J. Li, Manipulating interfacial charge redistribution in $Mn_{0.5}Cd_{0.5}S$/N-rich C_3N_5 S-scheme heterojunction for high-performance photocatalytic removal of emerging contaminants, *Journal of Materials Science & Technology*, 2026, **243**, 265-274, doi: 10.1016/j.jmst.2025.05.011.

[54] Z. L. Jin, Y. J. Li, H. R. Dong, S. J. Xiao, J. Y. Xiao, D. D. Chu, X. Z. Hou, S. X. Xiang, Q. X. Dong, L. Li, A comparative study on the activation of persulfate by mackinawite@biochar and pyrite@biochar for sulfamethazine degradation: The role of different natural iron-sulfur minerals doping, *Chemical Engineering Journal*, 2022, **448**, 137620, doi: 10.1016/j.cej.2022.137620.

[55] Y. Feng, P. H. Lee, D. L. Wu, K. M. Shih, Surface-bound sulfate radical-dominated degradation of 1,4-dioxane by alumina-supported palladium (Pd/Al_2O_3) catalyzed peroxymonosulfate, *Water Research*, 2017, **120**, 12-21, doi: 10.1016/j.watres.2017.04.070.

[56] J. Q. Wang, C. J. Wang, H. G. Guo, T. Ye, Y. Liu, X. Cheng, W. Li, B. Yang, E. D. Du, Crucial roles of oxygen and superoxide radical in bisulfite-activated persulfate oxidation of bisphenol AF: Mechanisms, kinetics and DFT studies, *Journal of Hazardous Materials*, 2020, **391**, 122228, doi: 10.1016/j.jhazmat.2020.122228.